

Assessment of the Importance of Mooring Dynamics on the Global Response of the DeepCwind Floating Semisubmersible Offshore Wind Turbine

Marco Masciola^a, Amy Robertson^a, Jason Jonkman^a, Alexander Coulling^b and Andrew Goupee^b

^aNational Renewable Energy Laboratory, Golden, CO, USA

^bAdvanced Structures and Composites Center, University of Maine, Orono, ME, USA

ABSTRACT

This paper studies the influence of mooring line dynamics on the response of a coupled floating offshore wind turbine against an equivalent uncoupled model. The semisubmersible modeled in this paper is based on a design developed by the DeepCwind program and uses the National Renewable Energy Laboratory's (NREL's) 5-megawatt (MW) baseline wind turbine to represent the tower, nacelle, and blade properties. The uncoupled model was formed using FAST, an open-source program that models the wind turbine aerodynamics, control, motion, tower/blade flexure, and wave forces, but with the mooring line forces treated using a quasi-static approximation. In contrast, the coupled model was enabled by pairing FAST with OrcaFlex. OrcaFlex replaces FAST's wave force and quasi-static cable model with an equivalent subsea fluid-structure representation and a lumped-mass cable system to capture the mooring line dynamics. This analysis revealed that an uncoupled model using the quasi-static mooring approximation can underestimate peak mooring line loads versus a coupled model using a dynamic mooring line.

KEY WORDS: Floating wind turbine; coupled analysis; semisubmersible; mooring dynamics

NOMENCLATURE

A_c	Column cross-section area
\mathbf{B}	6×6 quadratic drag matrix
C_D	Viscous (quadratic) drag coefficient
d_z	Mooring axial cable damping coefficient
EA	Mooring axial stiffness
$F_i(t)$	Wave excitation force
\mathcal{F}_i	Dimensionless wave-excitation force
H, H_s	Wave height, significant wave height
K_i	Linearized stiffness for the i^{th} DOF
$\tilde{k}(s)$	Elastic wave number (for the mooring line)
L	Unstretched cable length
q	Generalized platform displacement
T	Wave period
$\mathcal{T}(s)$	Cable tension power spectral density (PSD)
u	Local fluid velocity
$X_f(\omega)$	Wave excitation force at frequency ω
γ	Joint North Sea Wave Project (JONSWAP) spectrum peak enhancement factor
λ	Model/prototype scaling factor
μ	Cable mass per unit length
ω	Angular frequency (rad/s)

INTRODUCTION

Floating offshore wind turbines are viewed as a promising technology that has an ability to harness the large wind resource available in deep water. Recent studies show that offshore wind has the potential to help diversify worldwide energy resources and reduce dependency on hydrocarbons. As a result, there is a large drive to study how floating offshore wind turbines can supplement land-based wind resources. Fortunately, the budding offshore wind industry can leverage several decades of offshore oil and gas expertise to help grow the offshore wind area into a mature field.

To aid in the research and development of new floating offshore wind turbine design concepts, the National Renewable Energy Laboratory (NREL) modified FAST, an aero-elastic computer-aided engineering (CAE) tool, to simulate the response and dynamic loads of land-based, fixed offshore, and floating offshore wind turbines (Jonkman and Buhl, 2005). FAST is a validated, comprehensive simulation program that considers the aerodynamic loads, tower and blade deflections, blade pitch and nacelle yaw controls, gear box, and torque transfer between the rotor and generator with nonlinear models in the time domain. In the realm of offshore floating wind turbine modeling, additional loads must be included, such as wave-excitation loads, fluid added-mass, wave-radiation damping, drag arising from flow separation, and the mooring line restoring forces. High-fidelity simulation tools will assist the offshore wind industry in developing economically sound, competitive, and viable concepts capable of surviving variable ocean environmental conditions. Currently, FAST is in the process of being enhanced with features to allow greater modeling fidelity.

Study Motivation

The focus of this paper is to analyze the response of a coupled and uncoupled semisubmersible floating wind turbine, using the DeepCwind system as a surrogate, to study how the mooring line dynamics may influence the motion of these and similar structures, Figs. 1~2. Data from 1/50th-scale tank tests performed at the Maritime Research Institute Netherlands (MARIN) were used as a basis to understand the characteristics of a coupled and uncoupled numerical model. To better comprehend subtle differences between responses, three numerical models were included in the analysis. Each model used a variation of accepted theories to better quantify the important physics and response characteristics of the simulation and

were compared to results seen in the 1/50th-scale experiment.

In this paper, the terms ‘coupled’ and ‘uncoupled’ refer to the offshore industry definition of the mooring line representation (DNV, 2010; API, 1997). In the uncoupled analysis, the mooring line dynamics were decoupled from the floating vessel motion. Uncoupled theory usually consists of a quasi-static approximation of the mooring line restoring forces (Irvine, 1992; Wang, *et al*, 2010). In comparison, coupled analysis numerically integrates the mooring line equation of motion to formulate the mooring line dynamic response (Merchant and Kelf, 1973; Ketchman and Lou, 1975; Jefferys and Patel, 1982). Again, in this exercise, ‘coupled’ and ‘uncoupled’ refer to how the mooring was modeled.

Coupled and Uncoupled Model Description

FAST is a simulation tool that combines the tower motion, blade deflection, aerodynamic forces, and hydrodynamics loads into the platform equation of motion. Despite all these features, FAST is considered to be an ‘uncoupled’ model, in the sense that the mooring line restoring forces are presently solved using a quasi-static representation (Jonkman, 2007). A coupled model was developed by combining FAST with OrcaFlex using the *FASTlink* module to access the *OrcaFlexAPI* dynamically linked library. The *OrcaFlexAPI.dll* library is distributed with all current versions of OrcaFlex and allows external programs to access OrcaFlex functions. Through the combination of FAST and OrcaFlex, a coupled model is produced. OrcaFlex itself is a time-domain program capable of modeling the cable dynamics and hydrodynamic loads of floating offshore vessels (Orcina, 2011). The mooring line dynamic loads include fluid-drag and added-mass, internal damping, and cable/seabed contact. Cable bending and torsion effects are omitted in both the FAST and FAST+OrcaFlex simulations. The specific code-coupling mechanisms are further explained in Masciola, *et al* (2011); but for completeness, the authors define the fundamental assumptions in creating the FAST+OrcaFlex coupled model briefly in this paper.

The FAST+OrcaFlex coupled model combines the two programs to exploit the strengths of both modeling tools. FAST models the aerodynamic load and considers atmospheric turbulence on the blades, tower-bending moments, blade deflection, and wind turbine control algorithms. OrcaFlex is well-known for its dynamic mooring line representation and sophisticated hydrodynamic modeling utility that can model a multimember floating support structure as discrete elements. This permits each submerged column and cross brace to be modeled with different drag and added-mass coefficients. The two programs are combined in a manner that allows FAST to model the wind turbine components and OrcaFlex to model the floating vessel forces. OrcaFlex requires from FAST the platform displacement and velocity as input at the current time step to solve the mooring line and hydrodynamic forces. Once solved, the sum forces are returned to FAST, where the vessel acceleration is integrated within FAST, resulting in the subsequent time-step platform displacement and velocity.

The floating platform properties are defined in Table 1 (Robertson, *et al*, 2012; Coulling, *et al*, 2013). The wind turbine tower, blades, control algorithm, and gear box ratio were based on the NREL 5-megawatt (MW) baseline turbine for offshore systems (Jonkman, *et al*, 2007); however, modifications were made to the baseline wind turbine tower, blade, and nacelle values to match the 1/50th-scale model properties (Coulling, *et al*, 2013). The wave conditions analyzed in this paper are defined in Table 2. The first seven cases were compared to data recorded in the MARIN tests to explain

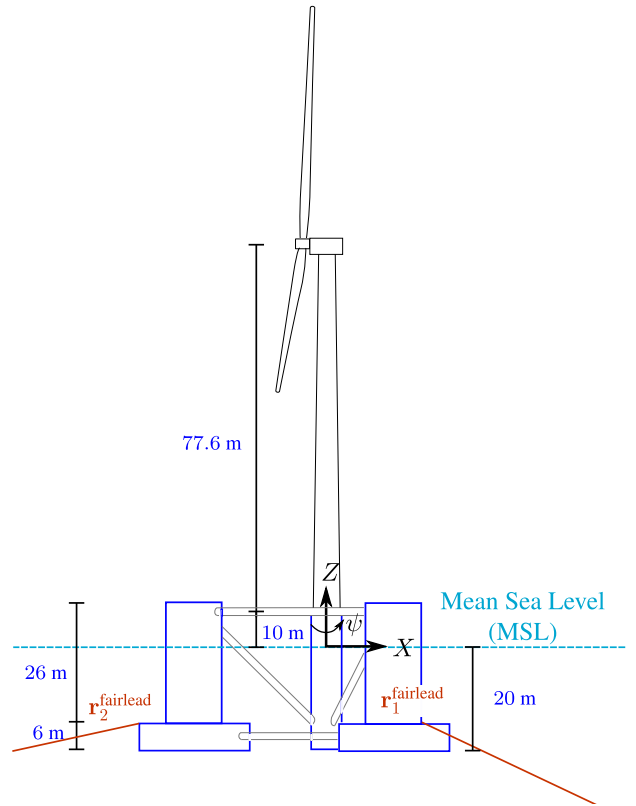


Fig. 1: Side profile of the DeepCwind semisubmersible floating wind turbine concept. The *XYZ* coordinates represent the reference origin of the DeepCwind platform. All coordinates reported in this manuscript are with respect to the platform reference origin. The platform six degrees-of-freedom motion are defined as surge (*X*), sway (*Y*), heave (*Z*), roll (ϕ), pitch (θ), and yaw (ψ).

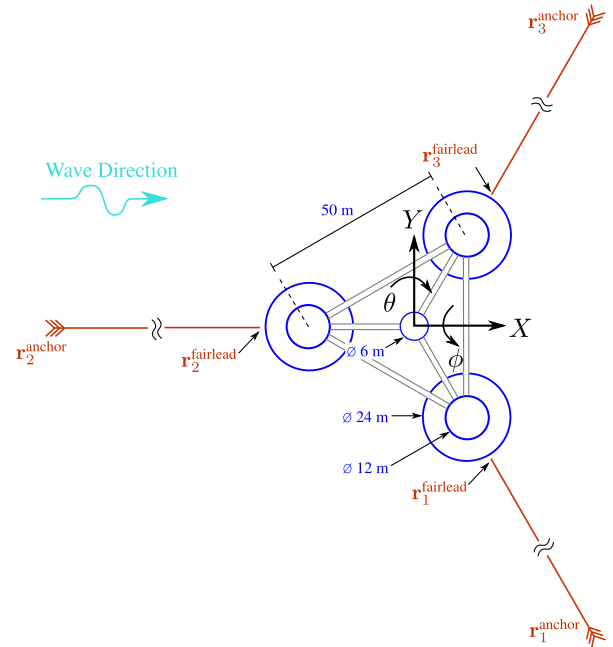
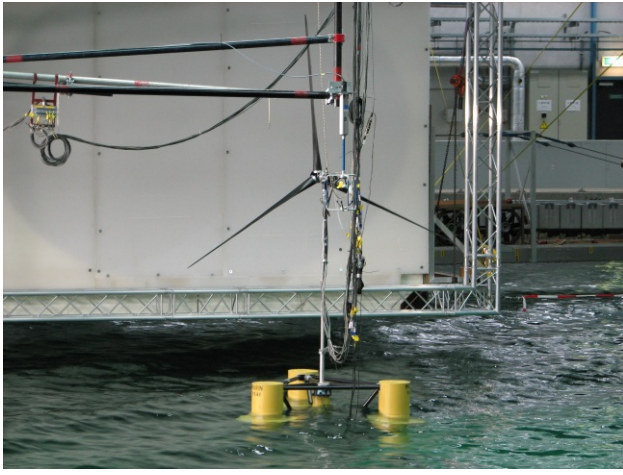


Fig. 2: Plan profile of the DeepCwind semisubmersible floating wind turbine concept. For all simulation and tank data results presented, the direction of wave propagation is aligned with the platform *X* direction.



(a)



(b)

Fig. 3: The 1/50th-scale DeepCwind semisubmersible model test performed at the Maritime Research Institute Netherlands (MARIN).

Table 1: Definition of the full-scale properties of the DeepCwind semisubmersible.

Rotor Diameter	126 m
Floating Platform Mass - M_{tot}	13.444×10^6 kg
Nacelle Mass - M_N	3.971×10^5 kg
Tower Mass - M_T	3.022×10^5 kg
Platform Center of Mass - C_M	-14.4 m
Platform Inertia at C_M - I_{XX}, I_{YY}	8.011×10^9 kg·m ²
Platform Inertia at C_M - I_{ZZ}	1.391×10^{10} kg·m ²
Platform Displacement - ∇	13.986×10^3 m ³
Mooring Axial Stiffness - EA	753.6×10^6 N
Unstretched Mooring Line Length - L	835.5 m
Mooring Mass Density - μ	113.352 kg/m
Structural Damping (OrcaFlex) - C_v	2.0% (stiffness proportional)
Seabed Friction Coefficient - C_B	1.0
Cable Drag Coefficient - C_d	1.15
Cable Added-Mass Coefficient - C_a	1.0
Mooring 1 Fairlead Position- $\mathbf{r}_1^{\text{fairlead}}$	$[20.43; -35.39; -14.00]^T$ m
Mooring 1 Anchor Position- $\mathbf{r}_1^{\text{anchor}}$	$[418.80; -725.38; -200.00]^T$ m
Mooring 2 Fairlead Position- $\mathbf{r}_2^{\text{fairlead}}$	$[-40.87; 0.00; -14.00]^T$ m
Mooring 2 Anchor Position- $\mathbf{r}_2^{\text{anchor}}$	$[-837.60; 0.00; -200.00]^T$ m
Mooring 3 Fairlead Position- $\mathbf{r}_3^{\text{fairlead}}$	$[20.43; 35.39; -14.00]^T$ m
Mooring 3 Anchor Position- $\mathbf{r}_3^{\text{anchor}}$	$[418.80; 725.38; -200.00]^T$ m

Table 2: Definition of the wave environments modeled. All cases assume a water density of 1025 kg/m³, no wind, and a parked rotor.

	Wave Amplitude [m]	Wave Period [s]	Spectrum
Case 1	$H = 7.58$	$T = 12.10$	Monochromatic
Case 2	$H = 10.30$	$T = 12.10$	Monochromatic
Case 3	$H = 7.14$	$T = 14.30$	Monochromatic
Case 4	$H = 10.74$	$T = 14.30$	Monochromatic
Case 5	$H = 7.57$	$T = 20.00$	Monochromatic
Case 6	$H = 11.12$	$T = 20.00$	Monochromatic
Operational 1	$H_s = 7.04$	$T_{avg} = 12.18$	JONSWAP, $\gamma = 2.20$
Operational 2	$H_s = 12.00$	$T_{avg} = 19.00$	JONSWAP, $\gamma = 2.20$

phenomena experienced in the basin and to compare with results acquired during the simulation. The final case labeled ‘Operational 2’ was viewed as a severe sea-state case and was simulation-only. This case was designed to exacerbate differences between the coupled and uncoupled numerical models. All cases were run with no wind present and the direction of wave propagation was aligned with the platform X direction (Fig. 2). This excited the platform in the surge (X), heave (Z), and pitch (θ). For brevity, the pitch results are not presented in this manuscript. Surge and heave results are sufficient to assess the coupled and uncoupled model characteristics for the DeepCwind system.

MODEL DEFINITION

This section breaks down the assumptions built into each numerical model analyzed in this paper. Each numerical model was developed using full-scale properties of the system, except for the viscous drag coefficients, which were implemented at model scale. The numerical models included are: 1) a standalone uncoupled FAST simulation using the \mathbf{B} drag matrix (Coulling, *et al.*, 2013), 2) the FAST+OrcaFlex coupled model with a consistent implementation of Morison’s equation to model the platform viscous forces, and 3) a FAST+OrcaFlex coupled model with the \mathbf{B} drag matrix to replace the discrete Morison element representation. The three numerical models were compared to the MARIN experimental tests. A brief description of the MARIN 1/50th-scale model follows first.

MARIN Tank Data Test

A 1/50th-scale Froude model based on the DeepCwind design was tested at the MARIN wave basin facility. The wind turbine tower, nacelle, rotor blade mass, and geometry were constructed to complement NREL’s 5-MW reference floating wind turbine (Jonkman, *et al.*, 2007); however, the tower, rotor, and nacelle designed for the 1/50th-scale model deviated from the reference turbine because of sensor mass (Robertson, *et al.*, 2012; Coulling, *et al.*, 2013). Scaling issues associated with the discrete placement of sensors along the tower were resolved by developing tower properties for the numerical models to match those used in the wave tank experiment. The floating platform was based on the full-scale representation of the DeepCwind system, but at 1/50th-scale, as pictured in Figs. 3(a)~3(b). Details regarding the scaled dimensions, mass and inertia, mooring line properties, and volumetric displacement for the complete system can

be found in Table 1 and in Coulling, *et al.*, (2013), with the scaling laws defined in Chakrabarti (1994). Though the results performed in the MARIN DeepCwind experiment were represented at model scale, all results depicted in this paper are amplified to full scale.

FAST with Quadratic Drag Matrix

An uncoupled representation of the floating system was constructed in FAST using the full-scale DeepCwind properties defined in Table 1. Included in this model are the effects of hydrodynamic loads associated with frequency-dependent added-mass, radiation damping, and the wave-excitation loads; all of which are solved in the frequency domain using the potential-flow solver WAMIT (Lee and Newman, 2006). The mooring line restoring force was calculated using a quasi-static approximation, thus forming the basis for our uncoupled model. The FAST model includes a quadratic drag matrix to approximate nonlinear flow separation forces not captured in potential theory. Because FAST was not equipped to model drag on multimember floating support columns at the time this analysis was performed, an equivalent drag matrix is derived based on MARIN tank test free-decay tests. This damping is based on the following mathematical formulation:

$$F_v^{\text{FAST}}(t) = -\mathbf{B} |\dot{\mathbf{q}}| \dot{\mathbf{q}} \quad (1)$$

where the drag matrix \mathbf{B} is defined as:

$$\mathbf{B} = \begin{bmatrix} 1.25E6 & 0 & 0 & 0 & 0 & 0 \\ 0 & 0.95E6 & 0 & 0 & 0 & 0 \\ 0 & 0 & 3.88E6 & 0 & 0 & 0 \\ 0 & 0 & 0 & 3.35E10 & 0 & 0 \\ 0 & 0 & 0 & 0 & 3.35E10 & 0 \\ 0 & 0 & 0 & 0 & 0 & 1.15E10 \end{bmatrix} \quad (2)$$

which is based on the study in Coulling, *et al.*, (2013). The vector $\dot{\mathbf{q}} = \{\dot{X}, \dot{Y}, \dot{Z}, \dot{\phi}, \dot{\theta}, \dot{\psi}\}^T$ is the six degree-of-freedom platform velocity. The units for Eq. 2 are Ns/m (for translational damping entries) and Nm-s/rad (for rotational damping entries). This damping is representative of a system at model scale. Mismatches in the viscous-drag coefficients between a model and full-scale system often occur in Froude models. Recall, as the scaling factor λ decreases ($\lambda = 50$ for the 1/50th-scale system), the error in the Reynold's number between the full-scale system and model also decreases (Chakrabarti, 1994):

$$\frac{\{\text{Re}\}_{\text{Full scale}}}{\{\text{Re}\}_{\text{Model scale}}} = \lambda^{2/3} \quad (3)$$

Given that drag coefficients are largely driven by the Reynold's number, they are difficult to match between full scale and model scale. These scaling issues are rectified by using model-scale drag coefficients in the simulation. In other words, model-scale drag coefficients are used when running the FAST and FAST+OrcaFlex simulations, even though the DeepCwind properties are implemented for a full-scale system.

FAST+OrcaFlex Coupled (A) Model

The FAST+OrcaFlex coupled model combines the wind turbine modeling features of FAST with the hydrodynamic and dynamic mooring line attributes of OrcaFlex. In OrcaFlex, each platform column and cross-brace is modeled as a discrete Morison element. Each individual component is given a unique drag coefficient based on its diameter and average Reynold's number. The WAMIT-derived potential forces account for radiation, wave excitation, hydrostatic

stiffness, and added-mass. To avoid double counting added-mass and fluid inertia, the acceleration terms in Morison's equation are omitted, effectively reducing it to a drag-only formulation. The column and cross-brace viscous drag models on each element of the DeepCwind column/pontoon element is (Abbott and Price, 1994; Orcina, 2011):

$$F_v^{\text{OrcaFlex}}(t) = \frac{1}{2} \rho C_D A_c |u - \dot{q}| (u - \dot{q}) \quad (4)$$

where C_D and A_c vary depending on the column diameter. The drag coefficients at model scale are:

- Diameter = 25 m, $C_D = 0.80$
- Diameter = 12 m, $C_D = 0.95$
- Diameter = 6 m, $C_D = 0.93$
- Diameter = 1.6 m, $C_D = 0.63$
- Heave plate = 4.80 (for $D = 25$ m column)

Of particular importance is the heave-plate drag coefficient, which is fixed at 4.80. The base of the outer support columns contribute significant damping to the system in both heave and in roll/pitch.

FAST+OrcaFlex Coupled Model (B) with Quadratic Damping Matrix

A second FAST+OrcaFlex coupled model was assembled to bridge gaps in theories between the uncoupled FAST model and the coupled FAST+OrcaFlex (A) simulation. This third simulation removes the Morison viscous-drag elements in the FAST+OrcaFlex (A) model, and replaces it with the \mathbf{B} damping matrix from Eqs. 1~2. The potential forces (i.e., the added-mass, radiation-damping, wave-excitation, and hydrostatic forces) retain their original formulation used in the other two numerical models. The idea is for this model to link our understanding between the FAST+OrcaFlex (A) model and the FAST-only model. This is instrumental in revealing subtle, yet important, properties about the models. By crafting a second FAST+OrcaFlex model that shares characteristics between the other two, the ambiguity of the results is reduced and allows one to isolate common features among the models. These results allow us to pinpoint differences to: 1) variations in how the hydrodynamic representation is implemented, and 2) the mooring line dynamics.

BASELINE SIMULATIONS

For baseline comparisons and to understand fundamental differences between the models, simulations were run for the three numerical models in monochromatic (regular) waves, as defined by the first six cases in Table 2. Equivalent tests were performed on the DeepCwind model at the MARIN test facility to provide a basis of comparison. These tests were intended to help quantify how well the models agree, reveal areas where expected differences may appear in subsequent simulations, and determine the role of mooring lines dynamics in the system response. The results of simulated regular wave tests against the MARIN tank test experiment are provided in Fig. 4. The bar charts were formed by measuring the response oscillation amplitude and dividing it by the wave amplitude. This produces a response amplitude operator, or RAO (St. Denis and Pierson, 1950). Each simulation was run for 1100 seconds to arrive at the steady-state oscillation amplitude values.

The Effect of Mooring Dynamics in Regular Waves

In Figs. 4(a) and 4(b), the surge and heave RAOs are shown. The line tension RAOs at fairleads 1 and 2 are depicted in Figs 4(c) and 4(d). The x-axis 'cases' are organized from left to right in order of

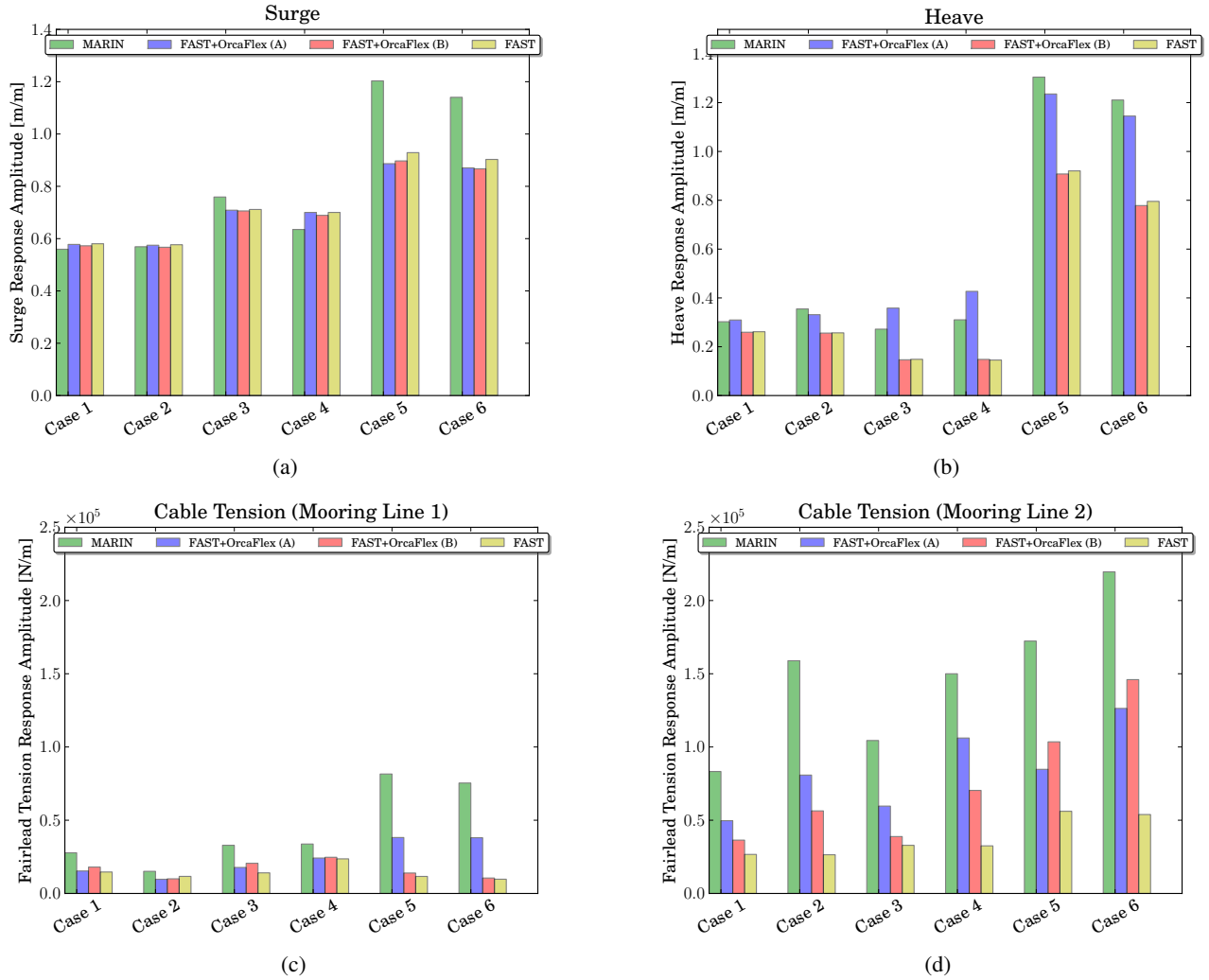


Fig. 4: From top-left, counter-clockwise: the RAOs for regular wave cases defined in Table 2 for surge, fairlead tension 1, fairlead tension 2, and heave.

increasing wave period. Each wave period is paired with two different wave heights (Table 2). Although the pair of wave heights are different for each frequency, the RAOs in surge, Figs. 4(a), and heave, Figs. 4(b), both scale proportionally to wave height; this relationship demonstrates nearly linear behavior (St. Denis and Pierson, 1950). Another trend noticed in Fig. 4(b) is that the FAST+OrcaFlex (A) heave RAO overshoots the response measured in the other data sets for cases 3 and 4 ($T = 14.30$ s).

The FAST+OrcaFlex (A) model, which uses a consistent implementation of Morison's equation, shows how including the relative velocity term ($u - q$) in the viscous force calculation can affect the response. The FAST+OrcaFlex (A) model compared better with the MARIN tank test data in the heave direction than the other two formulations using the **B** matrix. The drag forces on the heave plates are increased because the fluid velocity u fluctuates at frequencies near the DeepCwind heave resonance frequency.

The tension RAO in 4(d) does not scale proportionally to wave height as well as the displacement RAOs. The partial differential equation describing the dynamics for a cable demonstrates both spatial and temporal dependency (French, 1971); whereas the platform displacement RAOs can be reduced to a function of one variable

(namely, the wave height). This sensitivity to boundary conditions makes it difficult to characterize the tension RAO according to wave height alone. Because fairlead 2 is oriented parallel to the direction of wave propagation, Fig. 2, it experiences greater peak loads than the remaining two tendons.

There is a noticeable difference between the uncoupled (FAST) and coupled (FAST+OrcaFlex) tensions; this degree of variance is within the realm of what is considered reasonable for coupled and uncoupled models based on the assessment in Kwan and Bruen (1991) and API RP 2SK (2005). The tension RAO in mooring line 1 shows greater consistency between all numerical models; however, discrepancies between the two FAST+OrcaFlex models occurs for case 5 and case 6 (where the wave period is $T = 20.00$ seconds). These differences appear to be localized at this excitation frequency, but the exact cause is undetermined. Further study is needed to disclose the cause. One of the main observations noted in this regular wave study is that the vessel displacement RAOs remain approximately the same at different wave heights with the same period, but the tension RAO can vary by a wide margin.

IRREGULAR WAVES

The special case of irregular waves is considered in the next two simulated cases. The first set of operational wave conditions will be compared to MARIN data. A follow-up simulation was performed for a platform in rough seas. The second irregular case presented illustrates a special case showing the significance of the mooring line dynamics in the system response. The second case was not run for the MARIN 1/50th-scale test.

Operational Case 1 ($H_s = 7.04$ m, $T_{avg} = 12.18$ s)

Operational Case 1 illustrates the response of the DeepCwind system in irregular seas using the spectrum defined in Table 2. The time series plots in Figs. 5(a), 5(c), and 5(e) all show a reasonable level of agreement between the surge and heave response for the three simulation models and one MARIN tank-test. Accompanying each time series is the corresponding power spectral density (PSD) plot to its right. The data set also shows agreement within the wave-band frequencies (i.e., the region between 0.05–0.20 Hz) in Figs. 5(b), 5(d), and 5(f). Differences at the low frequency range in the surge and tension plot between the simulations and tank test can be attributed to second-order hydrodynamic effects not captured in the three numerical models (Coulling, *et al.*, 2013). Figure 4(b) shows that the uncoupled FAST and coupled FAST+OrcaFlex (B) agree with one another, and this is likely due to both models incorporating identical damping matrix representations through Eq. 1. The alternative FAST+OrcaFlex (A), the one which uses a consistent Morison representation of the viscous forces, Eq. 4, shows greater response at low surge frequencies.

The tension PSD plot for fairlead 2 in Fig. 5(f) shows significant differences between the MARIN results and the three numerical models. Although the tension amplitudes vary by a large degree, they do not impact the DeepCwind displacements compared to the simulations. The sharp, trochoidal peak appearing at 1.67 Hz is a result of the longitudinal (axial) cable natural frequencies. The longitudinal cable natural frequencies are a function of the cable length L , the cable mass per length, and the cable's axial stiffness. The n^{th} vibration mode can be estimated analytically (French, 1971):

$$f_n^u = \frac{n}{2L} c_z = \{1.54, 3.08, 4.62\} \text{ Hz} \quad (5)$$

where $c_z = [EA/\mu]^{1/2}$ is the longitudinal wave speed in units of meters per second. Typically, only coupled models utilizing a lumped-mass, finite-element analysis (FEA), or finite-differencing decomposition of the mooring line forces are capable of capturing longitudinal cable vibrations. There are more rigorous analytical solutions that are capable of modeling these effects (Irvine, 1991); however, these sophisticated catenary models are not implemented in FAST, thus the longitudinal spikes are not representable in FAST. The longitudinal peak in Fig. 5(f) for the two coupled models does not coincide with the calculated solution of 1.54 Hz because a portion of the mooring line is laying on the seafloor, and this is not represented in the boundary conditions that derived Eq. 5 (French, 1971).

A significant discrepancy at the longitudinal frequency between the MARIN data and FAST+OrcaFlex simulations exists. These peaks can be exaggerated from the numerical scheme coupling FAST and OrcaFlex, or it can be attributed to the numerical model being precise enough to capture the real dynamics of the test environment. A large difference exists between the three numerical models and the wave tank data at the peak wave frequency in Fig. 5(f). One explanation for this discrepancy could be because the mooring system

was geometrically scaled to match the full-scale stiffness values, but the dynamic (inertia) properties were not scaled accordingly. For example, Eq. 5 is not uniform between the model and full-scale values (Idichandy and Bhattacharyya, 2004).

Operational Case 2 ($H_s = 12.00$ m, $T_{avg} = 15.00$ s)

The plots in Fig. 6 illustrate the DeepCwind semisubmersible response in a larger sea-state. The researchers found the surge and heave responses to agree in both time, Figs. 6(a) and 6(c), and frequency, Figs. 6(b) and 6(d), within the wave-band frequencies. Because the FAST and FAST+OrcaFlex (B) models match in the heave PSD in Fig. 6(d), differences in those plots and FAST+OrcaFlex (A) model are associated with the manner in which the viscous damping term was formulated. The difference in the formulation of Eq. 1 versus Eq. 4 does not appreciably impact the surge motion, but has a perceptible involvement in shaping the heave response. This difference is likely attributed to the significance of heave plate drag coefficient ($C_D=4.80$) and because the wave orbital velocity u oscillates at a rate near the heave natural frequency. The inclusion of a dynamic mooring line representation does not appear to affect the global motion in the surge or heave directions. One mechanism of measuring the relative importance of a given sea-state on the global motion of a floating platform is through the dimensionless wave force coefficient (Masciola, *et al.*, 2013):

$$\mathcal{F}_i = \frac{F_i(t)}{K_i H_s} \quad (6)$$

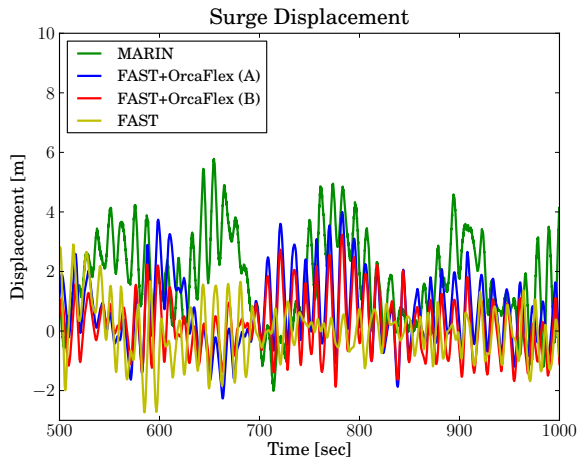
The linearized stiffness coefficient K_i considers the effective stiffness of the mooring line (and not buoyancy); the linearized stiffness in surge K_X and heave K_Z are 7.09×10^4 N/m and 1.91×10^4 N/m, respectively (Robertson, *et al.*, 2012). Likewise, $F_i(t)$ represents the wave-excitation load as a function of time. For simplicity, $F_i(t)$ is reduced to the root-mean-square of the wave-excitation force time series. Once all entities are substituted into Eq. 6, the following results are obtained:

- $\mathcal{F}_X^{\text{Operational 1}} = 11.61$
- $\mathcal{F}_X^{\text{Operational 2}} = 9.58$
- $\mathcal{F}_Z^{\text{Operational 1}} = 15.21$
- $\mathcal{F}_Z^{\text{Operational 2}} = 17.53$

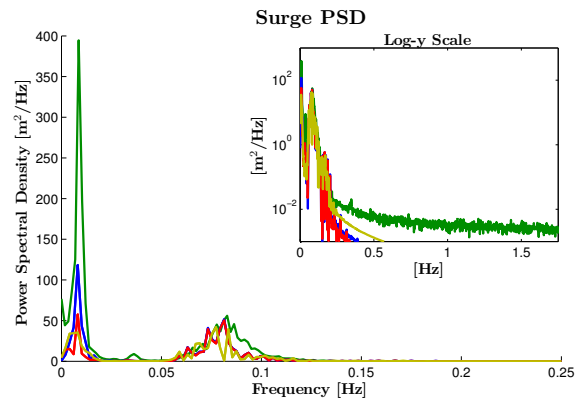
The nondimensional wave force magnitudes do not vary significantly between sea-states, which highlights that the platform motion will show similar characteristics in its response to wave forces between Operational Case 1 and Operational Case 2.

Differences between the coupled and uncoupled models are shown in the tension time-series plot, Fig. 6(e) and its corresponding PSD plot, Fig. 6(f). In multiple instances, both FAST+OrcaFlex models experienced line loads greater than those anticipated by the uncoupled FAST model. On a few occasions, the fairlead experienced a loss in tension, such as at $t = 923$ seconds, for the FAST+OrcaFlex (A) model. At this instance, a snap load ensued, and the uncoupled platform experienced greater heave motion than its coupled counterpart, suggesting that the mooring line dynamics impart short-duration, localized differences.

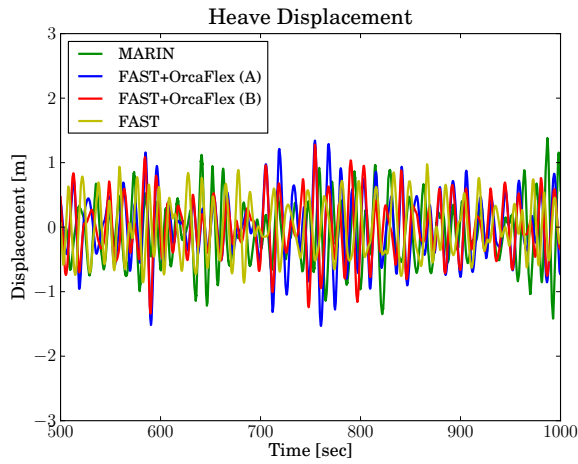
Another nondimensional parameter—the dimensionless mooring line tension—shows that mooring line peak tensions scale proportionally to platform displacement in the frequency domain. In dimensional form, the equation is (Masciola, *et al.*, 2013):



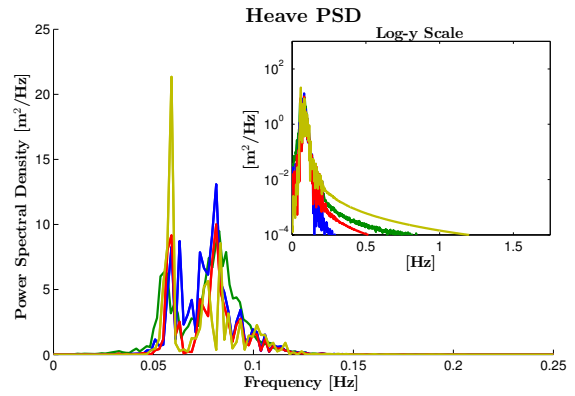
(a)



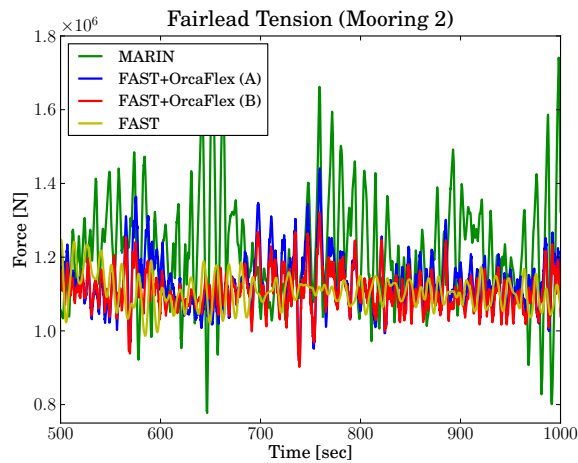
(b)



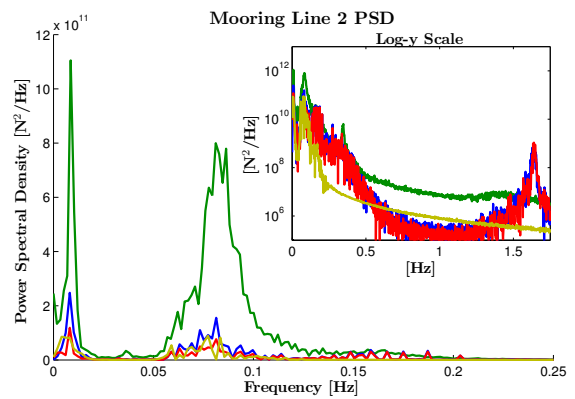
(c)



(d)

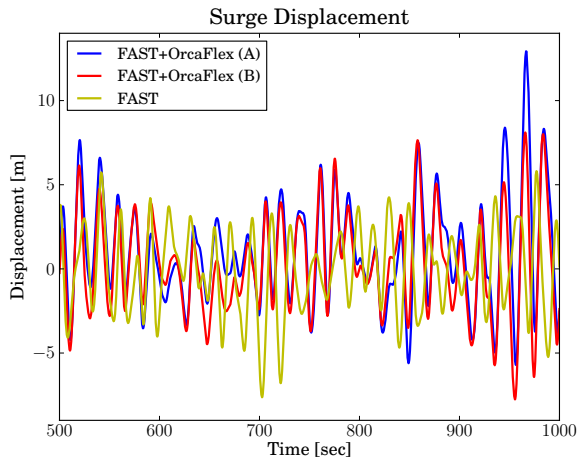


(e)

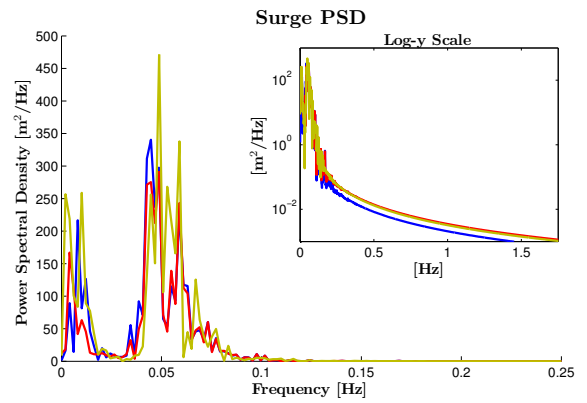


(f)

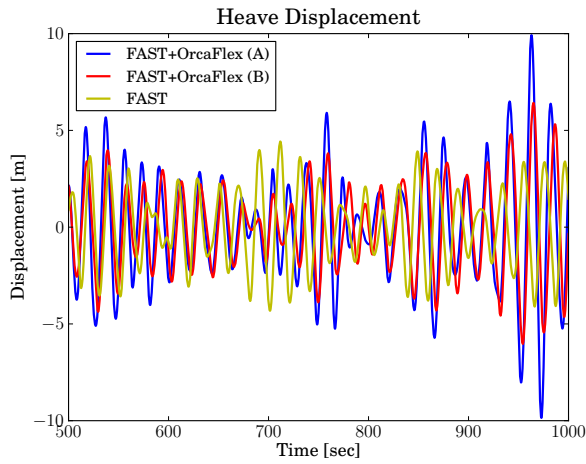
Fig. 5: Illustration of the platform surge (a) and heave (c) time series for Operational Case 1, Table 2. The fairlead tension in mooring line 2 is pictured in (e). The corresponding power spectral density (PSD) plots are shown to the right of the time-series plots. The small inset plot in (b), (d), and (f) shows the power spectrum across a broader frequency range.



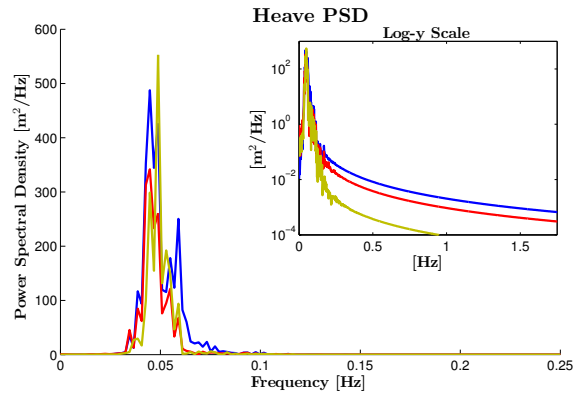
(a)



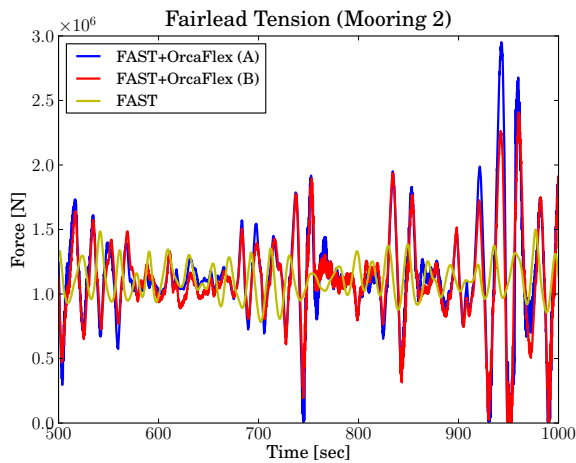
(b)



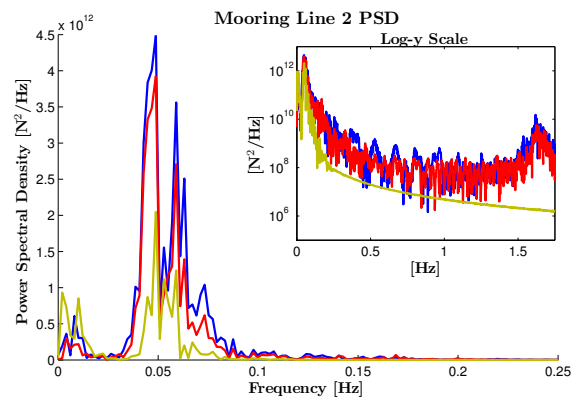
(c)



(d)



(e)



(f)

Fig. 6: Illustration of the platform surge (a) and heave (c) time series for Operational Case 2, Table 2. This example demonstrates a case where the platform tension varies drastically between the coupled and uncoupled numerical models. The small inset plot in (b), (d), and (f) shows the power spectrum across a broader frequency range.

$$T(s) \propto \frac{EA\tilde{k}}{L \tanh(\tilde{k})} q(s) \quad (7)$$

where $q(s)$ is the power spectrum of the platform displacement and \tilde{k} is the dimensionless elastic mooring line wave number:

$$\tilde{k} = \sqrt{s^2 + s \frac{Ld_z}{\mu c_z}} \quad (8)$$

where $s = j\omega$. The variable \tilde{k} exists because of the natural dynamics of the mooring line (i.e., it captures the longitudinal cable vibrations in Eq. 5). We find that the variance in the mooring line tension increases as the floating platform motion $q(s)$ increases. As the sea-state grows, so will the value for $q(s)$. Equation 7 highlights the relationships that exist between the platform properties and environment parameters when assessing the importance of the mooring line dynamics. For most floating offshore systems, there is an implicit relationship between the left-hand side of Eq. 7 and $q(s)$, which makes it difficult to predict the role of the mooring line dynamics in the platform response as a whole.

ASSESSMENT OF MOORING DYNAMICS ON PLATFORM MOTION AND CONCLUSION

This paper discusses the significance of mooring line dynamics on the loads of a semisubmersible floating offshore wind turbine using the DeepCwind geometry as a surrogate of study. To develop the coupled semisubmersible model, FAST is combined with OrcaFlex to capture the dynamics of the mooring lines. The results in this paper also consider an uncoupled model using FAST and MARIN tank test data for a 1/50th-scale Froude model subjected to equivalent sea-states. In total, one experiment and three simulation models were compared with one another. Differences between the three numerical models and one wave tank model were observed in irregular wave cases. These differences are largely attributed to:

- 1) Discrepancies in how the hydrodynamics model was implemented.
- 2) The mooring representation (uncoupled analysis versus coupled analysis).
- 3) The absence of second-order hydrodynamic effects in the numerical models (Coulling, *et al.*, 2013).
- 4) The inability of the numerical models to capture the full characteristics of the wave tank model.

The quasi-static mooring line used in the uncoupled FAST model does not model cable dynamics, which explains the large differences observed in the tension plots in Figs. 6(e)~6(f) and RAO studies shown in Fig. 4(d).

A key finding in this paper is that the mooring line dynamics have a limited role in influencing the surge and heave semisubmersible motion, but are significant when observing the tendon tension in extreme sea-states. For low sea-states, the uncoupled model provides acceptable levels of fidelity in modeling the platform motion for the six regular and one irregular wave cases studied. However, this model breaks down in larger sea-states, where the effects of mooring line inertia, added-mass, and drag tend to overwhelm the static forces/mean cable tensions. Another observation the researchers noted in this paper during the course of this investigation concerns extreme tension loads, especially at the onset of a snap load. When snap loads occur, the coupled and uncoupled platform responses differ. The duration between a loss of cable tension and a snap load is short,

but is important enough to affect the outcome of the results. A snap load results in a large force being applied to the platform due to rapid cable retensioning, and this reaction explains why large differences occur between the coupled and uncoupled models in regions near snap loads. The prediction of extreme loads is an important issue when evaluating the survivability of a particular offshore floating wind turbine design.

The findings in this paper are generally geometry-, platform-, and sea-state-dependent, and should not be used to characterize or interpret the response of other semisubmersibles. Further studies are needed to ascertain exact instances and environments when mooring line nonlinearities and inertia are important. As Eq. 7 suggests, the importance of the mooring line dynamics is difficult to diagnose, as the force is dependent on platform displacement, which is largely driven by sea-state conditions. An important finding of this work suggests that the mooring loads calculated using a quasi-static model may underpredict the dynamic response of a cable in extreme event situations as well as in regular wave conditions.

ACKNOWLEDGMENTS

This research was funded by the U.S. Department of Energy's Wind and Water Power Program.

REFERENCES

- Abbott, MB, and Price, WA (1994). *Coastal, Estuarial and Harbour Engineer's Reference Book*, Taylor & Francis, New York, New York, USA.
- API Recommended Practice 2T (1997). *Recommended Practices for Planning, Designing, and Constructing Tension Leg Platforms*, American Petroleum Institute, 254 pp.
- API Recommended Practice 2SK (2005). *Design and analysis of stationkeeping system for floating structures, Third Edition*, American Petroleum Institute.
- Chakrabarti, SK (1994). *Offshore Structure Modeling*. World Scientific Press, River Edge, New Jersey, USA, 470 pp.
- Coulling, AJ, Goupee, AJ, Robertson, AN, Jonkman, JM, and Dagher, HJ (2013). "Validation of a FAST semisubmersible floating wind turbine model with DeepCwind test data." *Journal of Renewable and Sustainable Energy*, in review.
- Det Norske Veritas (DNV) (2010). *Recommended Practice: Global Performance Analysis of Deepwater Floating Structures*, DNV-RP-F205, 28 pp.
- French, AP (1971). *Vibrations and Waves*, W.W. Norton and Company, New York, NY, USA.
- Idichandy, JA, and Bhattacharyya, VG (2004). "Experimental and Numerical Study of Coupled Dynamic Response of a Mini Tension Leg Platform," *Journal of Offshore Mechanics and Arctic Engineering*, Vol. 125, pp. 318-330.
- Irvine, M (1992). *Cable Structures*. Dover Publications, 272 pp.
- Jefferys, ER, and Patel, MH (1982). "On The Dynamics of Taut Mooring Systems," *Engineering Structures*, Vol. 4, No. 1, pp. 37-43.
- Jonkman, JM, and Buhl Jr., ML (2005). *FAST User's Guide*, NREL Technical Report, NREL/EL-500-29798.
- Jonkman, JM (2007). *Dynamics Modeling and Loads Analysis of an Offshore Floating Wind Turbine*, NREL Technical Report, NREL/EL-500-41958, 208 pp.
- Jonkman, JM, Butterfield, S, Musial, W, and Scott, G (2007). *Definition of a 5-MW Reference Wind Turbine for Offshore System Development*, NREL Technical Report No. TP-500-38060.
- Ketchman, JJ, and Lou, YK (1975). "Application of the Finite Element Method to Towed Cable Dynamics," Proceedings of MTS/IEEE OCEANS '75, Los Angeles, California, USA. Vol. 1, pp. 98-107.
- Kwan, CT, and Bruen, FJ (1991). "Mooring Lines Dynamics: Comparison of Time Domain, Frequency Domain, and Quasi-Static Analysis," 23rd Annual Offshore Technology Conference (OTC), May 6-9, Houston, Texas, USA. Vol 3, Paper No. 6657, pp. 95-109.

- Lee, CH, and Newman, JN (2006). *WAMIT User Manual, Versions 6.4, 6.4PC, 6.3S, 6.3S-PC*, WAMIT, Inc., Chestnut Hill, Massachusetts, USA.
- Masciola, MD, Robertson, A, Jonkman, J, and Driscoll, FR (2011). "Investigation of a FASTOrcaFlex Coupling Module for Integrating Turbine and Mooring Dynamics of Offshore Floating Wind Turbines," *International Conference on Offshore Wind Energy and Ocean Energy*, Oct. 31 - Nov. 2, Beijing, China.
- Masciola, MD, Nahon, M, and Driscoll, FR (2013). "Preliminary Assessment of the Importance of Platform-Tendon Coupling in a Tension Leg Platform," *Journal of Offshore Mechanics and Arctic Engineering*, In Press.
- Merchant, HC, and Kelf, MA (1973). "Non-Linear Analysis of Submerged Buoy Systems," *Proceedings of MTS/IEEE OCEANS 1973*, Vol. 1, pp. 390-395.
- Orcina, Ltd. (2012). *OrcaFlex Manual, Version 9.6a*, 474 pp.
- Robertson, A, Jonkman, J, Masciola, MD, Song, H, Groupee, A, Coulling, A, and Luan, C (2012). *Definition of the semisubmersible Floating System for Phase II of OC4*, NREL Technical Report, Golden, Colorado, USA.
- St. Denis, M, and Pierson, WJ (1950). "On the Motion of Ships in Confused Seas," *SNAME Transactions 61*, pp. 280-332.
- Wang, L, Guo, Z, and Yuan, F (2010). "Quasi-Static Three-Dimensional Analysis of Suction Anchor Mooring System," *Ocean Engineering*, No. 37, pp. 1127-1138.